Meccanica (2021) 56:2293–2305
https://doi.org/10.1007/s11012-021-01358-8

Dynamic analysis of a belt transmission with the GMS friction model

Krzysztof Kubas · Andrzej Harlecki

Received: 14 May 2020 / Accepted: 15 April 2021 / Published online: 12 May 2021

Abstract The paper presents a certain method of analysing the dynamics of a belt transmission. A flat transmission model developed by us was presented. For the analysis, it assumed the transmission 5PK belt. A discrete belt model, being a system of rigid beams interconnected with flexible and shock-absorbing elements, was used. To account for the mutual influence between the belt and pulleys, the Kelvin–Voigt contact model was used. The GMS friction model was also implemented, which allows all basic known friction phenomena to be taken into account. For this purpose, the vector of generalized coordinates was expanded with additional sub-systems of coordinates modelling the flexible belt-pulley connection. Moreover, two additional cases of a sudden transmission start were presented: with values of driving and resistance torque not causing a significant slip in the transmission as well as values of torque that cause slip.

Keywords Dynamic analysis · Belt transmission · GMS friction model

K. Kubas (✉) · A. Harlecki
University of Bielsko-Biala, Willowa 2,
43-309 Bielsko-Biala, Poland
e-mail: kkubas@ath.bielsko.pl

A. Harlecki
e-mail: aharlecki@ath.bielsko.pl

List of symbols

n_{GMS}	Number of GMS bodies
x_{T_i}	Displacement of ith rigid body (RB) in global contact
$x_{T_{i,k}}$	Displacement of kth GMS element of ith RB
$T_{i,k}$	Value of friction force acting on kth GMS element of ith RB
$\Delta x_{T_{i,k}}$	Deformation of local friction contact k of ith RB
σ_k	Stiffness coefficient of local friction contact k
$N_{i,k}$	Value of normal reaction force in local frictional contact k of ith RB
N_i	Value of normal of reaction force in global frictional contact of ith RB
$\mu^*_{i,k}$	Computational friction coefficient in local contact k of ith RB
$\mu_{i,k}$	Friction coefficient in this contact
μ_C	Coulomb friction coefficient independent of slip velocities $\dot{x}_{T_i}$
μ_s	Static friction coefficient
v_S	Stribeck velocity
T_i	Value of friction force in global contact of ith RB
$\mathbf{P}_i$	Vector of ith RB position
$\mathbf{q}$	Vector of of generalized coordinates of transmission model
n_b	Number of rigid bodies
n_p	Number of pulleys
θ_j	rotation Rf jth pulley

$\mathbf{F}_i$	Force acting on ith RB from spring-damping elements (SDEs)
$\mathbf{R}_i$	Force acting on ith RB from pulleys
$\mathbf{F}_{gi}$	Gravity force of ith RB
$\mathbf{M}_i$	Torque acting on ith belt body
I_{zj}	Mass moment of inertia of jth pulley
M_j	Value of torque acting on jth pulley
$\mathbf{M}_{T_{i,j}}$	Torque from friction force of ith belt body
$\mathbf{v}_{i,j}$	Relative velocity between ith body and jth pulley

1 Introduction

Leonard Euler [1] was the first to initiate research on the phenomena occurring in belt transmission systems. The first paper discussing the existence of micro-displacements in belt transmissions was written by Reynolds [2]. The research objectives, which changed over the centuries together with some more important works, were presented by Fawcett in [3]. What also deserves a mention are papers in which friction between rubber and other materials was modeled. The most well-known examples include works related to automotive engineering, especially those dealing with the modelling of friction between the tire and the road, e.g. a frequently cited work by [4]. The proposed friction model, also presented in the paper above, included the Dahl friction model [5]. The paper [4] also introduced another dynamic friction model, the LuGre model, which allows accounting for the Stribeck effect. Belt models can be divided into continuous models where the belt is modeled as an elastic rod [6] or a string with some longitudinal stiffness and sometimes with bending stiffness [7–10], and discrete [11–14] models, most commonly assuming rigid beam elements joined together by translational and sometimes additionally by torsional spring-damping elements.

The papers [13, 14] presented belt transmission models with a linear friction model with the possibility of predicting belt creep. This is called the Coulomb-like tri-linear creep-rate-dependent friction model. In [15], a model taking into account the elastic/perfectly-plastic friction law (EPP) was presented.

What also deserves a mention is a group of papers in which the Dahl friction model is applied as a way of modelling friction in the revolute joint in a belt tensioner, e.g. [16, 17].

In his papers, the authors developed two-dimensional models of belt transmissions using the Dahl friction model [18], the Threlfall friction model [19], and a model that included a microslip [20]. In [20], the assumptions and requirements made during the process of model development were presented.

The Generalized Maxwell-Slip friction model (hereinafter referred to as GMS friction model) was used to take into account the friction between the belt and the pulleys of the belt transmission under consideration. The application of the GMS friction model to the belt transmission model is a novel approach to the problem. The GMS model has been developed as an expansion of the Leuven friction model [21, 22] and the earlier LuGre model [23], in turn, based on the Dahl model. The GMS friction model has been described in several basic publications, which are chronologically [24–27]. This is a universal model, as it allows to take into account all known friction phenomena i.e. preliminary displacement (first described in [28]), together with the interdependence between the static friction coefficient and the tangential loading rate [29, 30] and hysteresis with non-local frictional memory [31, 32], the Stribeck effect (for the first time described in [33]) and the phenomenon of time delay in the case of dynamic friction characteristics (described for the first time in [34]). Because of these properties, the analysed model may be successfully used for the analysis of the "stick-slip" phenomenon occurring in various mechanical systems, including belt transmissions.

The stick-slip phenomenon occurring in belt transmissions was analysed, among others, in [35–38].

2 Method of dynamic analysis

2.1 Application of the generalized Maxwell-slip friction model to account for friction between the belt and pulleys of the belt transmission

To analyse the presented friction model, it is necessary to consider the system of n_{GMS} bodies presented in Fig. 1 and known from physics. It is a system of interconnected parallel, weightless Maxwell elements [39, 40].

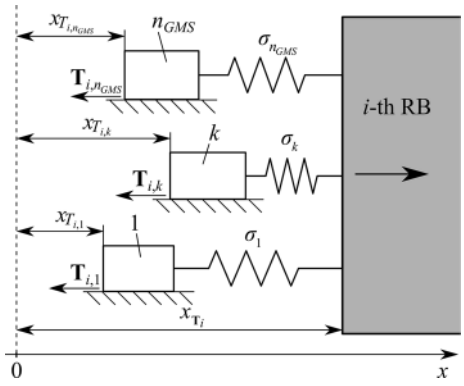

Fig. 1 Maxwell's system of elements

For considerations presented in this paper Maxwell's elements correspond to local frictional contacts at the places where individual unevenness of the surfaces sliding on top of each other interact. These surfaces constitute contact surfaces for the individual discrete rigid element modelling the belt together with relevant pulleys. These elements move in such a way that the slip phase under kinetic friction conditions is separated by a short-term standstill phase under static friction conditions.

The input value for the system under consideration is the displacement x_{T_i} in the global contact under consideration. Element k, where $k = 1, \ldots, n_{GMS}$ (its number is equivalent to the number of the relevant local frictional contact), whose displacement is determined by the coordinate $x_{T_{i,k}}$, has its own individual initial value $T_{i,k}$ of the friction force acting on it.

As shown in the Fig. 1, positive or negative spring deformation k is determined by the formula:

$$\Delta x_{T_{i,k}} = x_{T_i} - x_{T_{i,k}}, \tag{1}$$

with the spring deformation $\Delta x_{T_{i,k}}$ (representing the state variable) being equivalent to the deformation of the local friction contact k modeled by the spring in the direction tangential to the direction of movement.

The value $T_{i,k}$ of the friction force acting on the element k, equivalent to the force exerted by in by the spring under consideration, with either positive or negative sign, is proportional to the change $\Delta x_{T_{i,k}}$:

$$T_{i,k} = \sigma_k \Delta x_{T_{i,k}}, \tag{2}$$

where the spring coefficient of stiffness σ_k is the same as the coefficient of the stiffness of the local friction contact k modelled by it in a direction tangential to the direction of movement. This coefficient takes the same value, regardless of the rigid body (RB) considered.

Taking into account Coulomb's formula, the value of the friction force acting on element i can be expressed as:

$$T_{i,k} = \mu^*_{i,k} N_{i,k}, \tag{3}$$

where $N_{i,k}$—value of normal reaction force in the local frictional contact k under consideration.

The value of $N_{i,k}$ can be expressed as:

$$N_{i,k} = v_k N_i, \tag{4}$$

where N_i—the value of the normal of the reaction force in global frictional contact i, i.e. contact of the discrete rigid element i with the relevant pulley, v_k—weight coefficient meeting $\sum_{k=1}^{n_{GMS}} v_k = 1$.

The computational friction coefficient $\mu^*_{i,k}$ in the local frictional contact k under consideration is expressed by the formula:

$$\mu^*_{i,k} = \mathrm{sgn}\dot{x}_{T_i} \mu_{i,k}, \tag{5}$$

where $\mu_{i,k}$—friction coefficient in this contact (taking the same value regardless of the RB under consideration).

Taking into account the relations (2) and (3), the computational friction coefficient can be presented as:

$$\mu^*_{i,k} = \sigma_{\mu_k} \Delta x_{T_{i,k}}, \tag{6}$$

with the following coefficient being taken into account:

$$\sigma_{\mu_k} = \frac{\sigma_k}{N_{i,k}}. \tag{7}$$

If element k stays immobile, then the following condition is met:

$$\dot{x}_{T_{i,k}} = 0, \tag{8}$$

thus, based on formula (1) it may be written:

$$\Delta \dot{x}_{T_{i,k}} = \dot{x}_{T_i}. \tag{9}$$

If element k stays in motion, the differential equation expressing the time derivative of the computational friction coefficient is true:

$$\frac{d\mu^*_{i,k}}{dt} = \mathrm{sgn}\dot{x}_{T_i} v_k c \left(1 - \frac{\mu^*_{i,k}}{s(\dot{x}_{T_i})}\right), \tag{10}$$

where c—attraction parameter, expressed in s^{-1}, determining the convergence speed of the computational friction coefficient $\mu^*_{i,k}$ to the value of the expression $s(\dot{x}_{T_i})$.

This equation was implemented after a slight modification of the original relationship presented in paper [25] in which there are values of friction forces and not its coefficients.

The expression $s(\dot{x}_{T_i})$, determining the course of the computational kinetic friction coefficient in the global contact i as a function of the constant slip velocities $\dot{x}_{T_i}$, is presented by a formula illustrating the so-called Stribeck effect (Fig. 2) taken from [41]. This formula has the form:

$$s(\dot{x}_{T_i}) = \mathrm{sgn}\dot{x}_{T_i}\left(\mu_C + (\mu_s - \mu_C)e^{-\left(\frac{\dot{x}_{T_i}}{v_S}\right)^2}\right), \tag{11}$$

where μ_C—Coulomb friction coefficient independent of the slip velocities $\dot{x}_{T_i}$, μ_s—static friction coefficient, v_S—Stribeck velocity.

Taking into account the relationship (6), (10) can be transformed into:

$$\Delta\dot{x}_{T_{i,k}} = \mathrm{sgn}\dot{x}_{T_i}\frac{v_k c}{\sigma_{\mu_k}}\left(1 - \frac{\mu^*_{i,k}}{s(\dot{x}_{T_i})}\right). \tag{12}$$

Variables $\Delta\dot{x}_{T_{i,k}}$ in any movement moment t are determined by integrating differential equations (9) and (12). Then, based on formula (6), computational friction coefficients $\mu^*_{i,k}$ can be determined.

The element k stays immobile as long as the condition $|\mu^*_{i,k}| \le |s(\dot{x}_{T_i})|$ is met, and it remains in motion as long as slip velocity $\dot{x}_{T_{i,k}}$ does not change its sign.

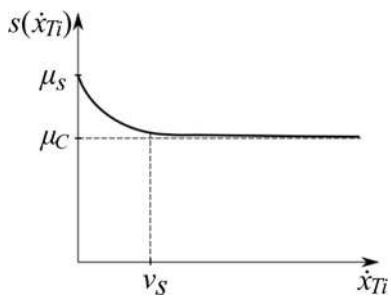

Fig. 2 Graphical representation of the expression $s(\dot{x}_{T_i})$ presenting Stribeck effect (for $\dot{x}_{T_i} > 0$)

Now, the value of friction force T_i in the global contact i under consideration can be calculated using the equation:

$$T_i = N_i \sum_{k=1}^{n_{GMS}} \mu^*_{i,k} v_k. \tag{13}$$

2.2 The model of transmission with discrete belt model

It assumed a discrete belt model, divided into n_b rigid bodies (RB) connected by spring damping elements (SDE) with longitudinal stiffness, damping and bending stiffness also being assumed. Every belt element, shown in Fig. 3, is described by the position vector:

$$\mathbf{P}_i = \begin{bmatrix} x_i \\ y_i \\ 0 \end{bmatrix}, \tag{14}$$

and the rotation θ_i. In the transmission model, it also assumed n_p pulleys.

The GMS model of friction with the number of n_{GMS} of the assumed bodies is connected with the ith belt body by spring elements. The vector of generalized coordinates can be therefore written as:

$$\mathbf{q} = \begin{bmatrix} \mathbf{q}_b & \mathbf{q}_p & \mathbf{q}_{GMS} \end{bmatrix}^T, \tag{15}$$

where $\mathbf{q}_b = \begin{bmatrix} x_1 y_1 \varphi_1 & \dots & x_i y_i \varphi_i & \dots & x_{n_b} y_{n_b} \varphi_{n_b} \end{bmatrix}^T$—vector of coordinates of n_b bodies, $\mathbf{q}_p = \begin{bmatrix} \theta_1 & \dots & \theta_j & \dots & \theta_{n_p} \end{bmatrix}^T$—vector of coordinates of n_p pulleys, $\mathbf{q}_{GMS} = \begin{bmatrix} \mathbf{q}_{1GMS} & \cdots & \mathbf{q}_{iGMS} & \cdots & \mathbf{q}_{n_bGMS} \end{bmatrix}^T$—vector of coordinates of all elements k,

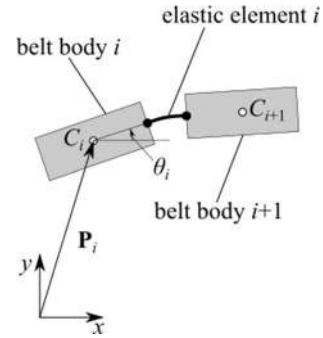

Fig. 3 Assumed belt bodies and spring damping element

$\mathbf{q}_{iGMS} = [\, z_{i,1} \quad \ldots \quad z_{i,k} \quad \ldots \quad z_{i,n_{GMS}} \,]^T$—vector of coordinates of element n_{GMS} connected to ith RB, $i = 1 \ldots n_b, j = 1 \ldots n_p, k = 1 \ldots n_{GMS}$.

The number of generalized coordinates can be therefore calculated with the formula: $n = 3n_b + n_p + n_b n_{GMS}$.

Coordinates of belt bodies can be derived from vector $\mathbf{q}$ in the following manner:

$$x_i = \mathbf{q}[3i-2], y_i = \mathbf{q}[3i-1], \varphi_i = \mathbf{q}[3i]. \tag{16}$$

Coordinates of pulleys can be also calculated from:

$$\theta_j = \mathbf{q}[3n_b + j]. \tag{17}$$

and also coordinates of elements k from:

$$z_{i,k} = \mathbf{q}[3n_b + n_p + (i-1) \cdot n_{GMS} + k]. \tag{18}$$

Equations of motion of belt bodies can be formulated as the following system:

$$\begin{cases} m_i \ddot{x}_i &= \hat{\mathbf{X}}^T (\mathbf{F}_i + \mathbf{R}_i + \mathbf{F}_{gi}) \\ m_i \ddot{y}_i &= \hat{\mathbf{Y}}^T (\mathbf{F}_i + \mathbf{R}_i + \mathbf{F}_{gi}) \\ I_{zi} \ddot{\varphi}_i &= \hat{\mathbf{Z}}^T \mathbf{M}_i \end{cases}, \tag{19}$$

where $\hat{\mathbf{X}}$—the unit vector along the x axis, $\hat{\mathbf{Y}}$—the unit vector along the y axis, $\hat{\mathbf{Z}}$—the unit vector along the z axis.

In the equations above, the vector $\mathbf{F}_i$ is the sum of forces from neighbouring spring-damping elements:

$$\mathbf{F}_i = \mathbf{F}_i^L + \mathbf{F}_i^R. \tag{20}$$

The vector $\mathbf{R}_i$ is the resultant reaction force acting from the pulleys:

$$\mathbf{R}_i = \sum_{j=1}^{n_p} (\mathbf{N}_{i,j} + \mathbf{T}_{i,j}), \tag{21}$$

where $\mathbf{N}_{i,j}$—the normal force between the ith belt body and the jth pulley, $\mathbf{T}_{i,j}$—the friction force between the ith belt body and the jth pulley.

The normal force $\mathbf{N}_{i,j}$ can be calculated from the formula:

$$\mathbf{N}_{i,j} = N_{i,j} \hat{\mathbf{r}}_{i,j}, \tag{22}$$

where $\hat{\mathbf{r}}_{i,j}$—the versor (unit vector) of the $\mathbf{r}_{i,j}$.

The vector $\mathbf{r}_{i,j}$ can be calculated from the formula:

$$\mathbf{r}_{i,j} = \mathbf{P}_i - \mathbf{P}_j^p, \tag{23}$$

where $\mathbf{P}_j^p$—position vector of the jth pulley.

The value of normal force $\mathbf{N}_{i,j}$ assumed from the same Kelvin–Voigt contact model as in [18]:

$$N_{i,j} = c_{con1} p_{i,j}^2 + c_{con2} p_{i,j} + b_{con} \dot{p}_{i,j}, \tag{24}$$

where $p_{i,j} = r_j - |\mathbf{r}_{i,j}|$, r_j—radius of the jth pulley, c_{con1}, c_{con1}—belt-pulley contact stiffness coefficients, b_{con}—belt-pulley contact damping coefficients.

The value of normal force N_i can be derived from:

$$\mathbf{N}_i = \sum_{j=1}^{n_p} \mathbf{N}_{i,j}. \tag{25}$$

The gravity force can be calculated from:

$$\mathbf{F}_{gi} = m_i \mathbf{g}, \tag{26}$$

where m_i—mass of the ith belt body.

The torque $\mathbf{M}_i$ acting on the ith belt body is the sum of torques from neighbouring spring-damping elements:

$$\mathbf{M}_i = \mathbf{M}_i^L + \mathbf{M}_i^R, \tag{27}$$

where

$$\mathbf{M}_i^L = \mathbf{M}_i^{Ltra} + \mathbf{M}_i^{Lben}, \tag{28}$$

$$\mathbf{M}_i^R = \mathbf{M}_i^{Rtra} + \mathbf{M}_i^{Rben}. \tag{29}$$

The components of the formulas presented above include translational and bending stiffness torques, from left and right spring-damping elements and can be calculated from:

$$\mathbf{M}_i^{Ltra} = -\mathbf{d}_i \times \mathbf{F}_i^L, \tag{30}$$

$$\mathbf{M}_i^{Rtra} = \mathbf{d}_i \times \mathbf{F}_i^R, \tag{31}$$

$$\mathbf{d}_i = \begin{bmatrix} \frac{l_i}{2} \cos \varphi_i \\ \frac{l_i}{2} \sin \varphi_i \\ 0 \end{bmatrix}. \tag{32}$$

The forces $\mathbf{F}_i^L = -\mathbf{F}_{i-1}^R$ have the same direction as the vector:

$$\mathbf{P}_i^{LR} = \mathbf{P}_i + \mathbf{d}_i - \mathbf{P}_{i-1} - \mathbf{d}_{i-1}, \tag{33}$$

whereas direction of the torques $\mathbf{M}_i^{Lben} = -\mathbf{M}_i^{Rben}$ conforms with the z axis. The values of these vectors can be calculated from:

$$F_i^L = F_{i-1}^R = c_{tra}\Delta l_i^L + b_{tra}\Delta l_i^L, \tag{34}$$

$$M_i^{Lben} = M_{i-1}^{Rben} = c_{ben}\Delta\varphi_i + b_{tra}\Delta\dot{\varphi}_i, \tag{35}$$

where $c_{tra} = \frac{n_b c_{tra}^b}{l}$, $b_{tra} = \frac{n_b b_{tra}^b}{l}$, $c_{ben} = \frac{n_b c_{ben}^b}{l}$, $b_{ben} = \frac{n_b b_{ben}^b}{l}$, $\Delta\varphi_i = \varphi_i - \varphi_{i-1}$, $\Delta\dot{\varphi}_i = \dot{\varphi}_i - \dot{\varphi}_{i-1}$, c_{tra}^b—translational stiffness per one unit length of the belt, b_{tra}^b—translational damping per one unit length of the belt, c_{ben}^b—bending stiffness per one unit length of the belt, b_{ben}^b—bending damping per one unit length of the belt, l—assumed length of the belt (calculated from geometric dependences).

The longitudinal deflection of the spring-damping elements can be calculated from:

$$\Delta l_i^L = \Delta l_{i-1}^R = P_i^{LR}. \tag{36}$$

Equations of motion of pulleys described as:

$$I_{zj}\ddot{\theta}_j = -M_j - \sum_{i=1}^{n_b} \hat{\mathbf{Z}}^T \mathbf{M}_{T_{i,j}}, \tag{37}$$

where $\mathbf{M}_{T_{i,j}} = \hat{\mathbf{r}}_{i,j} \times \mathbf{T}_{i,j}$—torque from friction force of ith belt body.

Components of the formula presented above have been shown in Fig. 4.

The relative velocity between the ith body and the jth pulley is:

$$\mathbf{v}_{i,j} = \mathbf{v}_{i,j}^p - \mathbf{v}_i^t, \tag{38}$$

where $\mathbf{v}_{i,j}^p = \hat{\mathbf{Z}} \cdot \dot{\theta}_j \times \hat{\mathbf{r}}_{i,j}$—the tangent pulley velocity vector, applied to the point of contact, $\mathbf{v}_i^t$—velocity vector of the ith belt body tangent to the pulley.

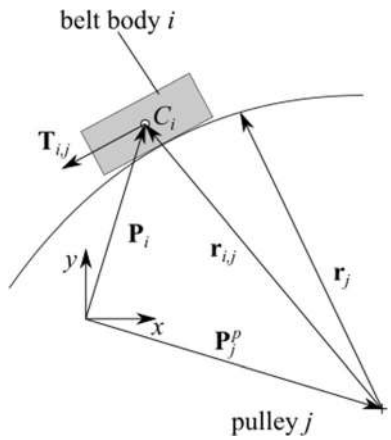

Fig. 4 The positions of the ith belt body and the jth pulley

The value of velocity $\mathbf{v}_i^t$ can be calculated from the following scalar product:

$$v_i^t = \mathbf{v}_i^T \cdot \mathbf{t}_{i,j}. \tag{39}$$

The direction of the vector $\mathbf{v}_i^t$ is the same as $\mathbf{t}_{i,j}$:

$$\mathbf{t}_{i,j} = \frac{\hat{\mathbf{Z}} \times \hat{\mathbf{r}}_{i,j}}{|\hat{\mathbf{Z}} \times \hat{\mathbf{r}}_{i,j}|}. \tag{40}$$

3 Results of simulations

For analysis, it assumed transmission with poly-V belt 5PK, presented schematically in Fig. 5. The transmission consists of two pulleys with identical radiuses equal to $r = 0.2$ m. The distance between the pulleys was $l = 1$ m. The centre of the first pulley was accepted as the origin of the system of coordinates O_1. It assumed that a driving torque of the arbitrary value of M_d will be applied to the first pulley and a resistance torque of M_{res} to the second pulley. Friction and contact parameters have been assumed based on data proposed in [42, 43]. The presented equations have been implemented in the C++ programming language. Runge–Kutta of the fourth order method was used for numerical integration of differential equations of motion. The multithreading of the processor was used to speed up the calculations, using the OpenMP library for this purpose. Table 1 presents the assumed parameter values.

3.1 First simulation

In the first analysed case, arbitrary drive torque values of $M_d = 20$ N m and resistance values of $M_{res} = 15$ N m were assumed. The course of the torques M_1 and M_2, acting on the pulleys have been assumed based on the following relations:

$$M_1 = \begin{cases} 50t & \text{for} \quad t = 0\ldots0.4\,\text{s}, \\ 20 & \text{for} \quad t = 0.4\ldots2\,\text{s}, \\ -50t + 120 & \text{for} \quad t = 2\ldots2.4\,\text{s}, \\ 0 & \text{for} \quad t > 2.4\,\text{s}. \end{cases} \tag{41}$$

$$M_2 = \begin{cases} 50t & \text{for} \quad t = 0\ldots0.3\,\text{s}, \\ 15 & \text{for} \quad t > 0.3\,\text{s}. \end{cases} \tag{42}$$

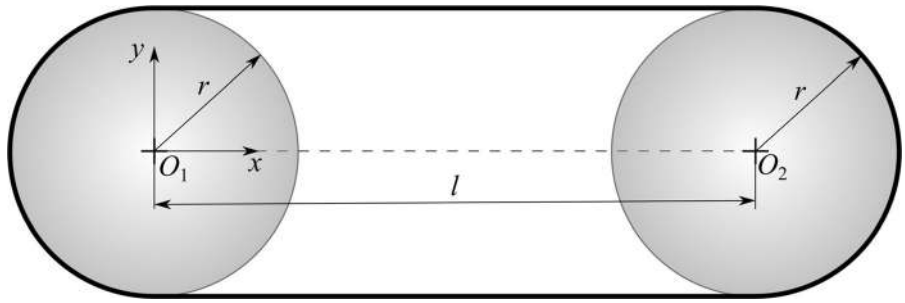

Fig. 5 The analysed transmission

Table 1 Assumed values of parameters

Parameter	Value	Unit
n_b	120	–
c_{tra}	50,000	N/m
b_{tra}	0.5	Ns/m
c_{ben}	0.0208	N/rad
b_{ben}	0	Ns/rad
n_{GMS}	3	–
σ_{μ_1}	1200	1/m
σ_{μ_2}	1600	1/m
σ_{μ_3}	2000	1/m
c	0.03	s^{-1}
v_k	$\frac{1}{3}$	–
μ_C	0.9	–
μ_s	1	–

As can be noticed from the formulas above, torque M_1 can achieve arbitrary value M_d ($t = 0.4 \ldots 2$ s,) whereas torque M_2 can achieve arbitrary value M_{res} ($t > 0.3$ s). Figure 6 presents the resulting course of torques M_1 and M_2 applied to the pulleys. Figure 7 presents the resulting angular velocities of the pulleys.

As can be seen with the resulting torque courses, until 0.3 s the values of these torques compensate. From this moment on, the torque M_1 dominates over torque M_2 and the transmission accelerates. From 2 s, the value of M_1 starts decreasing to reach zero at 2.4 s. As a result of this, the transmission starts decelerating. The simulation finishes when both pulleys come to a stop, i.e. after ca. 2.8 s.

Sudden start results in the generation of relatively large reaction forces in the belt and friction forces between the belt and the pulley. The transmission

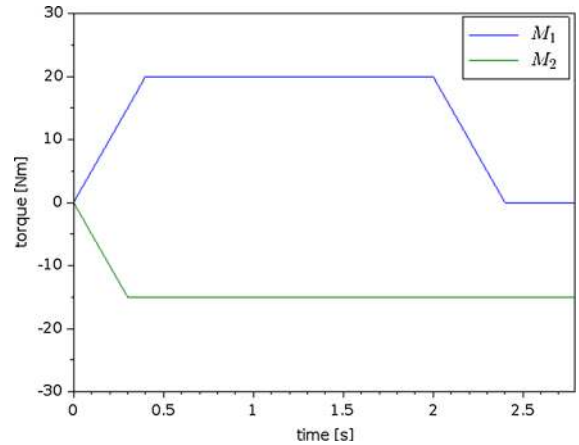

Fig. 6 The courses of drive and driven torque

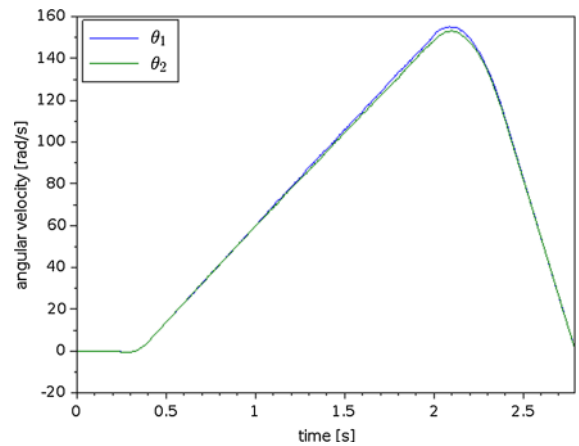

Fig. 7 The courses of angular velocities of drive and driven pulleys

deceleration is also quite sudden. Despite the sudden course of these torques in Fig. 7, no major differences between the angular velocity of the drive pulley and angular velocity of the driven pulley were observed,

which means that the transmission operates with only a slight slip. The transmission achieves its maximum velocity after ca. 2.1 s. At this moment, the angular velocity of the driven pulley is ca. 155 rad/s, whereas the angular velocity of the drive pulley is ca. 153 rad/s (slip was ca. 1.3%).

Figure 8 presents the course of normal force N_i acting on the selected ith RB. The zero values of this force mean that the selected ith RB is between the pulley in the tensioned or loose part of the belt.

Normal force directly influences the values of the friction force. The course of this force, for the same ith RB has been presented in Fig. 9. Figure 10 presents the resulting course of the reaction force in SDE directly neighbouring the analysed ith RB. Initially, this element is located on the driven pulley. At ca. 0.58 s, it moves towards the tensioned part of the belt between the driven and the drive pulley. The course presented in Fig. 10 clearly shows a significant increase in the reaction force in SDE. At ca. 0.76 s, repeated contact with a pulley, the drive pulley this time, takes place, which results in a quick drop in the reaction force. Then, at 0.83 s, the analysed ith RB separates from the pulley and moves along the loose part of the belt. Lower values of the reaction force are observed. Together with an increase in the pulley rotational speed, the transition phases between the driven pulley, tensioned part of the belt, drive pulley and lose part of the belt become increasingly shorter.

Figure 11 presents the values of friction forces calculated for each of the elements k. Figure 12, in turn, presents the corresponding value of the friction coefficient.

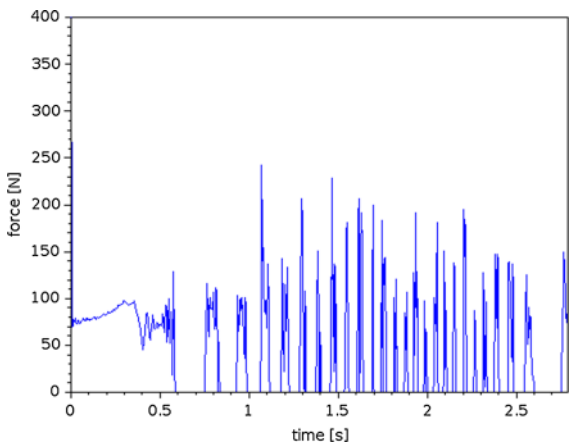

Fig. 8 The course of contact normal force N_i acting on selected ith RB from pulleys

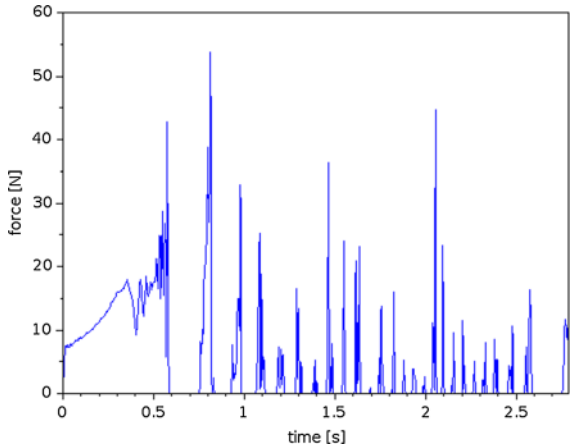

Fig. 9 The course of friction force T_i acting on selected ith RB from pulleys

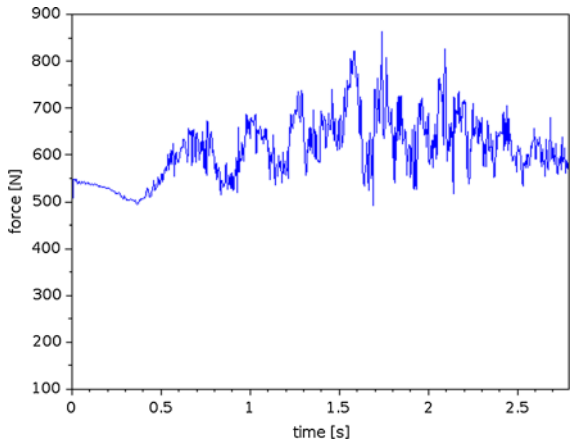

Fig. 10 The course of reaction force acting on selected ith RB from neighbouring SDE

Because the coefficient σ_{μ_1}, being the measure of stiffness, is the lowest, the calculated component of the friction force is also the lowest. Force values for elements $k = 2$ and $k = 3$ are proportionally larger. Insignificant disproportions between these force values may result from the fact that elements k do not move in synchrony.

The short-term drop in the value of these forces to zero at the moment of transmission start-up, although part of the belt with the analysed ith RB is located on the driven pulley, results from a temporary loss of adhesion ith RB (thus indirectly from relatively small flexibility of the assumed parameters of the contact

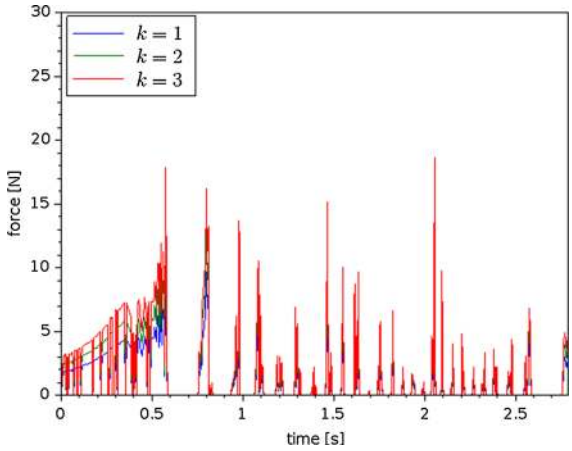

Fig. 11 The courses of friction force components calculated for elements k

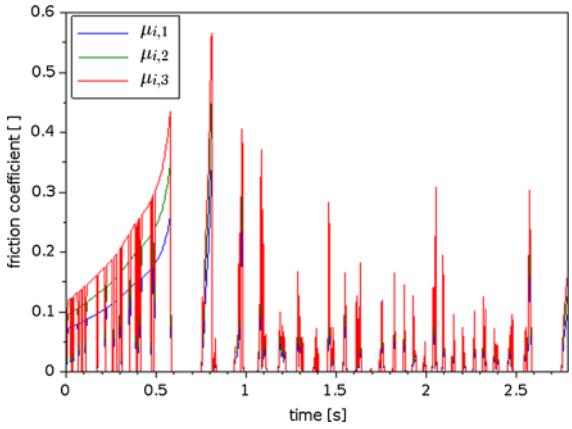

Fig. 12 The courses of friction coefficient values calculated for elements k

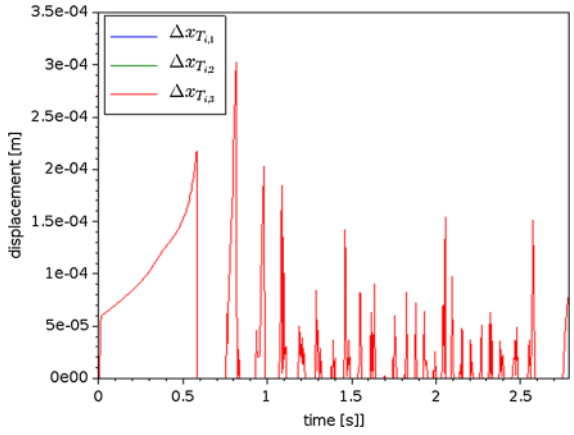

Fig. 13 The course of displacement $\Delta x_{T_{i,k}}$ of selected ith RB

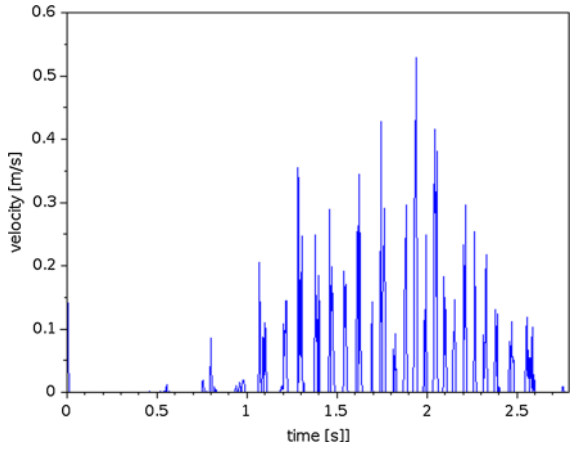

Fig. 14 The course of displacement velocity $\Delta \dot{x}_{T_{i,k}}$ of selected ith RB

model and the neighbouring SDE). It was also noted that the remaining neighbouring ith RB, which are also located on the pulley, do not detach from it in these moments.

In Fig. 12, it can be seen that the values of individual coefficients $\mu^*_{i,k}$ did not approach the arbitrary values of coefficients μ_s and μ_d.

Figures 13 and 14 present respectively the course of the displacement x_{T_i} and velocity $\dot{x}_{T_i}$ in friction connection between the analysed ith RB and the pulleys. As can be seen from the course presented in Fig. 13, the displacement values slightly exceed 3×10^{-4} m. The largest value is observed at first contact with the drive pulley, when the transmission accelerates. On the other hand, from Fig. 14, it can be concluded that the values of slip velocities are influenced by the rotational speed of the transmission and the values of drive torque and resistance. At the very moment when the disproportion between these elements is the greatest, just before the assumed reduction in drive torque, the largest velocity value of ca. 0.53 m/s was observed.

3.2 Second simulation

In the second analysed case, twice as large arbitrary values of the drive torque $M_d = 40$ N m and resistance $M_{res} = 30$ N m were assumed. Courses of the torques M_1 and M_2 were thus assumed to meet the following relations:

$$M_1 = \begin{cases} 100t & \text{for} \quad t = 0\ldots0.4\,\text{s}, \\ 40 & \text{for} \quad t = 0.4\ldots2\,\text{s}, \\ -100t + 240 & \text{for} \quad t = 2\ldots2.4\,\text{s}, \\ 0 & \text{for} \quad t > 2.4\,\text{s}. \end{cases} \tag{43}$$

$$M_2 = \begin{cases} 100t & \text{for} \quad t = 0\ldots0.3\,\text{s}, \\ 30 & \text{for} \quad t > 0.3\,\text{s}. \end{cases} \tag{44}$$

Figure 15 presents the resulting courses of torques M_1 and M_2 applied to the pulleys obtained in the second simulation. Whereas, Fig. 16 presents analogical resulting angular velocities of pulleys. As can be seen, at ca. 0.9 s, belt slip occurred. What is interesting is that this slip did not occur directly at the moment of achieving the maximum values of torques M_1 and M_2. Thus, without any doubt, an increase in the centrifugal force acting on the pulley also played a role. It increased under the influence of increasingly larger values of pulley angular velocities. Increasing values of this force lead to the reduction in normal force N_i. Maximum pulley angular velocities, in this case, were 835rad/s for the drive pulley and 102 rad/s for the driven pulley. Moreover, shortly after the occurrence of slip, the driven pulley reduced its speed close to zero. The simulation was interrupted once the drive pulley stopped.

Figures 17 and 18 present the resulting values of normal force N_i and friction T_i obtained for the second simulation. Comparing these courses with the base courses presented in Figs. 8 and 9, the previously mentioned reduction in the value of normal force together with a slight increase in friction force can be

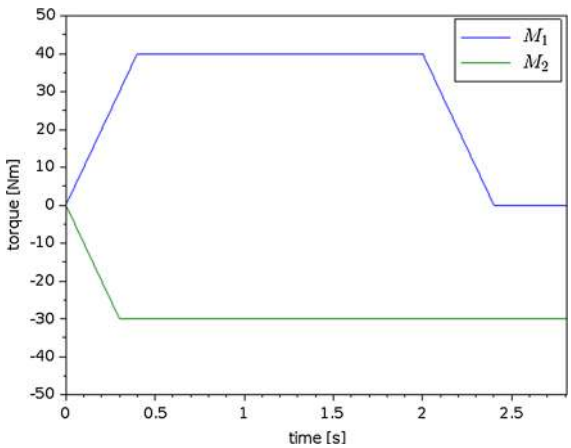

Fig. 15 The courses of drive and driven torque

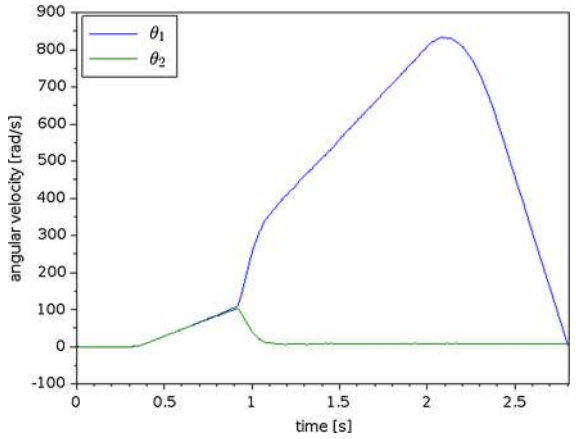

Fig. 16 The courses of angular velocities of drive and driven pulleys

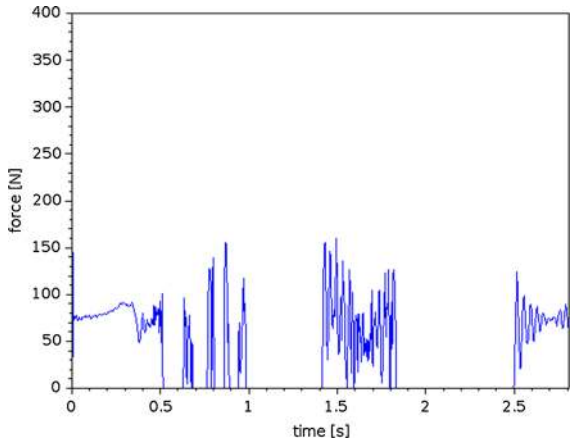

Fig. 17 The course of contact normal force N_i acting on selected *i*th RB from pulleys

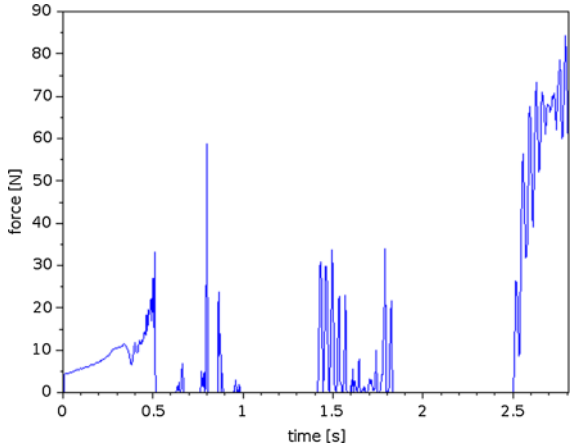

Fig. 18 The course of friction force T_i acting on selected *i*th RB from pulleys

observed, especially in the final phase of the simulation. After 2.5 s, the analysed *i*th RB slipped considerably on the driven pulley. At the previous stage, when the belt cooperated with the driven pulley (in the time interval ca. 1.41... 1.84 s) smaller friction values were observed as the belt was trying to follow the pulley.

When comparing the course of the reaction force in SDE presented in Fig. 19 with the course presented in Fig. 10, no major changes in the values of reaction forces in SDE neighbouring the analysed *i*th RB were observed.

Comparing the courses of friction forces for specific elements k presented in Fig. 20 with the courses presented in Fig. 11, the above-mentioned significant increase in friction force is also noticeable, but the disproportions between specific courses are smaller. The same short-lived moment when the *i*th RB detached from the driven pulley at the initial simulation stage was also observed. An analysis of the value of friction coefficients for specific elements k (Fig. 21) allows us to see that in the final transmission movement phase values close to μ_s and μ_d have been observed.

When analysing the course of the values $\Delta x_{T_{i,k}}$ (Fig. 22) and $\Delta \dot{x}_{T_{i,k}}$ (Fig. 23) at contact with the drive pulley (in time interval 1.41..1.84 s), relatively similar values of displacement of the individual elements k were observed. The reason for similar values includes the relatively large belt slip of ca. 141 m/s, which can be seen in the second course. Finally, when the analysed *i*th RB cooperates with the driven pulley,

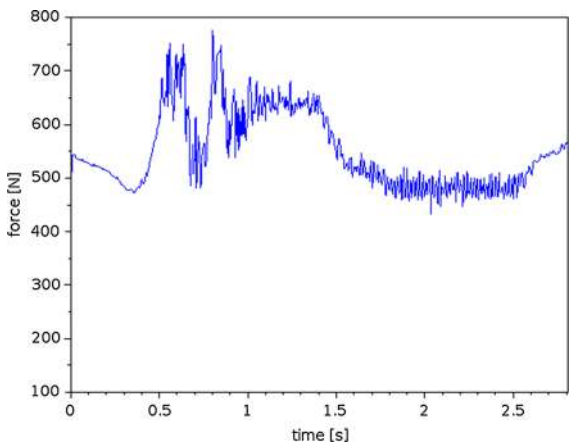

Fig. 19 The course of reaction force acting on selected *i*th RB from neighbouring SDE

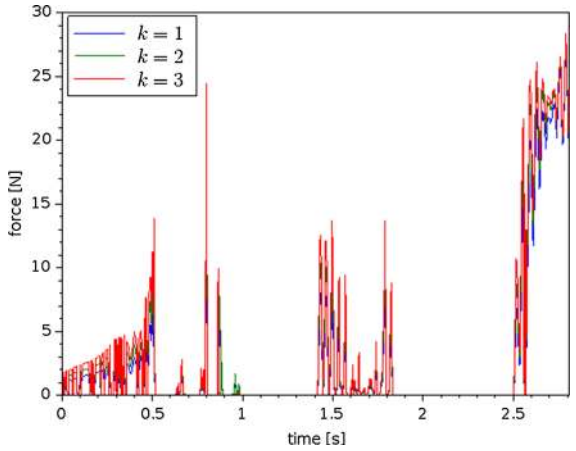

Fig. 20 The courses of friction force components calculated for elements k

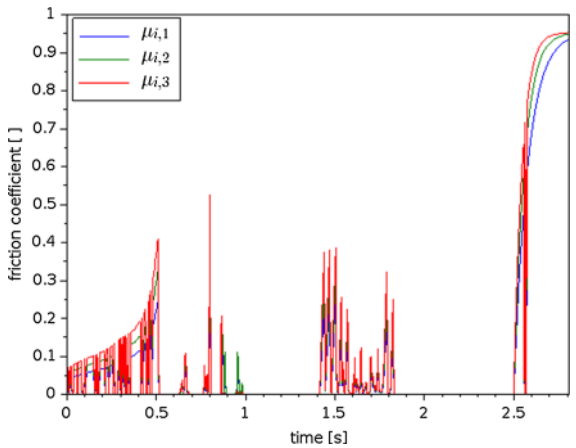

Fig. 21 The courses of friction coefficient values calculated for elements k

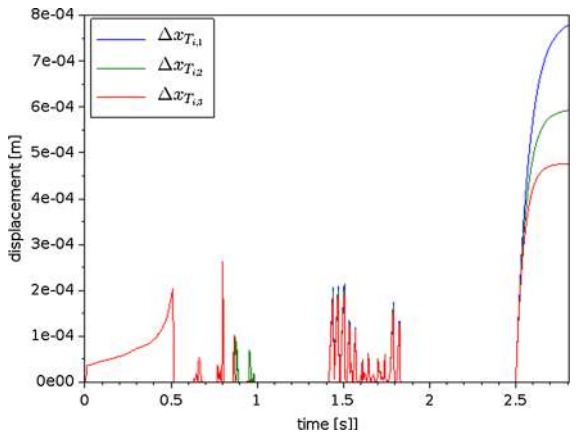

Fig. 22 The course of displacement $\Delta x_{T_{i,k}}$ of selected *i*th RB

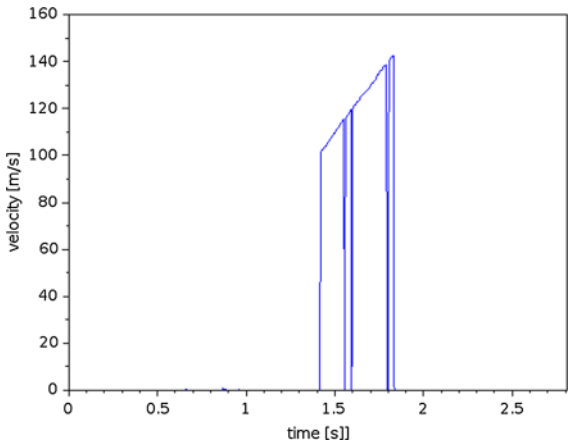

Fig. 23 The course of displacement $\Delta \dot{x}_{T_{i,k}}$ velocity of selected *i*th RB

the situation gets reversed. The values of displacement increase proportionally with each element k, and the slip becomes negligible.

4 Conclusions

As already mentioned, the GMS friction model, which takes into account all the basic known friction phenomena, allows for reflecting the continuous, i.e. the real nature of friction consisting in smooth, unnoticeable transmission from the phase of standstill (under static friction conditions) to phase of motion (under dynamic friction conditions) and the other way round. Similarly to earlier dynamic friction models such as the above-mentioned Dahl, LuGre, and Leuven models, this model is based on the same mathematical formulas regardless of the current phase. It constitutes a significant simplification of the computational process. This makes it different from the switching friction models, e.g. [44, 45], previously used in the dynamics of mechanical systems, where standstill and motion phases are analysed separately. Switching friction models are based on different mathematical formulas describing the friction phenomenon in both friction phases. This poses a major difficulty in the implementation of the computational process. It was necessary to develop a special control procedure allowing us to determine the transition conditions between the friction phases. It might lead to a hypothesis that despite using a complex mathematical apparatus, switching friction models becomes obsolete as they model both phases of friction separately thus failing to depict the continuous nature of friction. To achieve more realistic results in the future by using the GMS friction model, detailed identification of parameters of friction occurring in belt transmissions between the belt and the pulleys would be needed. It needs to be stressed that the GMS friction model is the latest and the most advanced of all the dynamic friction models used in the dynamics of mechanical systems but due to its complexity, it is hardly ever used in calculations. Therefore, in our opinion, this work, based on this model, may be perceived as truly novel.

Declarations

Conflict of interest The authors declare that they have no conflict of interest.

References

1. Euler ML (1762) Remarques sur l'effect du frottement dans l'equilibre. Mém Acad Sci, Berlin, pp 265–278
2. Reynolds O (1847) Creep theory of belt drive mechanics. Engineer 38:1847
3. Fawcett JN (1981) Chain and belt drives—a review. Shock Vib Digest 13(5):5–12
4. Canudas-de-Wit C, Tsiotras P, Velenis E, Basset M, Gissinger GL (2003) Dynamic friction models for road/tire longitudinal interaction. Veh Syst Dyn 39:189–226. https://doi.org/10.1076/vesd.39.3.189.14152
5. Dahl PR (1968) A solid friction model. The Aerospace Corporation, El Segundo, (CA), USA, T0R-0158(3107-18)-1
6. Belyaev AK, Eliseev VV, Irschik H, Oborin EA (2017) Contact of two equal rigid pulleys with a belt modelled as Cosserat nonlinear elastic rod. Acta Mech 228:4425–4434
7. Chowdhury S, Yedavalli RK (2016) Dynamics of belt-pulley-shaft systems. Mech Mach Theory 98:199–215
8. Oborin E, Vetyukov Y, Steinbrecher I (2018) Eulerian description of non-stationary motion of an idealized belt-

pulley system with dry friction. Int J Solids Struct 147:1–12. https://doi.org/10.1016/j.ijsolstr.2018.04.007
9. Dakel M, Jézéquel L, Sortais J-L (2018) Stationary and transient analyses of a pulley-belt system based on an Eulerian approach. Mech Mach Theory 128:682–707
10. Pan Y, Liu X, Shan Y, Chen G (2017) Complex modal analysis of serpentine belt drives on beam coupling model. Mech Mach Theory 116:162–177
11. Eliseev V, Vetyukov Y (2012) Effects of deformation in the dynamics of belt drive. Acta Mech 223:1657–1667
12. Julio G, Plante J-S (2011) An experimentally-validated model of rubber-belt CVT mechanics. Mech Mach Theory 46:1037–1053
13. Leamy MJ, Wasfy TM (2002) Analysis of belt-driven mechanics using a creep-rate-dependent friction law. Trans J Appl Mech ASME 69(6):763–771
14. Leamy MJ, Wasfy TM (2002) Transient and steady-state dynamic finite element modeling of belt-drives. ASME J Dyn Syst Meas Control 124(4):575–581
15. Kim D, Leamy MJ, Ferri AA (2011) Dynamic modeling and stability analysis of flat belt drives using an elastic/perfectly plastic friction law. ASME J Dyn Syst Meas Control 133:1–10. https://doi.org/10.1115/1.4003796
16. Bastien J, Michon G, Manin L, Dufour R (2007) An analysis of the modified Dahl and Masing models: application to a belt tensioner. J Sound Vib 302(4–5):841–864
17. Chatlet E, Michon G, Manin L, Jacquet G (2008) Stick/slip phenomena in dynamics: choice of contact model. Mech Mach Theory 43(10):1211–1224
18. Kubas K (2017) A model for the dynamic analysis of a belt transmission using the Dahl friction model. J Theor Appl Mech 55(4):1423–1435
19. Kubas K (2015) A model for analysing the dynamics of a belt transmissions with a 5pk belt. Arch Autom Eng 16(1):61
20. Kubas K (2014) A two-dimensional discrete model for dynamic analysis of belt transmission with dry friction. Arch Mech Eng 61(4):571–593
21. Swevers J, Al-Bender F, Ganseman CG, Prajogo T (2000) An integrated friction model structure with improved presliding behavior for accurate friction compensation. IEEE Trans Autom Control 45(4):675
22. Lampaert V, Swevers J, Al-Bender F (2002) Modification of the Leuven integrated friction model structure. IEEE Trans Autom Control. https://doi.org/10.1109/9.995050
23. Canudas de Wit C, Olsson H, Astrom KJ, Lischinsky P (1995) A new model for control of systems with friction. IEEE Trans Autom Control 40(3):419
24. Lampaert V, Al-Bender F, Swevers J (2003) A generalized Maxwell-slip friction model appropriate for control purposes. In: Proceedings of IEEE international conference on physics and control, Saint Petersburg, Russia
25. Al-Bender F, Lampaert V, Swevers J (2004) Modeling of dry sliding friction dynamics: from heuristic models to physically motivated models and back. Chaos. https://doi.org/10.1063/1.1741752
26. Al-Bender F, Lampaert V, Swevers J (2005) The generalized Maxwell-slip model: a novel model for friction simulation and compensation. IEEE Trans Autom Control. https://doi.org/10.1109/TAC.2005.858676
27. Al-Bender F, Swevers J (2008) Characterization of friction force dynamics. Behavior and modeling on micro and macro scales. IEEE Control Syst Mag. https://doi.org/10.1109/MCS.2008.929297
28. Rankin JS (1926) The elastic range of friction. Philos Mag 8(2)
29. Simkins TE (1967) The multuality of static and kinetic friction. Lubr Eng 23:26–31
30. Brockley CA, Davis HR (1968) The time dependence of static friction. Trans ASME J Lubr Technol 90:35–41
31. Courtney-Pratt JS, Eisner E (1957) The effect of a tangential force on the contact metalic bodies. Proc R Soc Lond Ser A 238:529–550
32. Mayergoyz ID (1991) Mathematical models of hysteresis. Springer, Berlin
33. Stribeck R (1902) Die wesentlichen Eigenschaften der Gleit- und Rollenlager. Zeitschrift des Vereines Deutscher Ingenieure, Bd.XXXVI, Nr.38
34. Sampson JB, Morgan F, Reed DW, Muskat M (1943) Studies in lubrication: XII. Friction behavior during the slip portion of the stick-slip process. J Appl Phys 14:689
35. Cheng G, Zu JW (2003) Nonstick and stick-slip motion of a coulomb-damped belt drive system subjected to multifrequency excitations. J Appl Mech 70:871–884
36. Frendo F, Bucchi F (2020) "Brush model" for the analysis of flat belt transmissions in steady-state conditions. Mech Mach Theory 143:103653
37. Frendo F, Bucchi F (2020) Enhanced brush model for the mechanics of power transmission in flat belt drives under steady-state conditions: effect of belt elasticity. Mech Mach Theory 153:103998
38. Sheng G, Lee JH, Narravula V, Song D (2011) Experimental characterization and analysis of wet belt friction and the vibro-acoustic behavior. Tribol Int 44:258–265
39. Lazan BJ (1968) Damping of materials and members in structural mechanics. Pergamon Press, London
40. Iwan WD (1966) A distributed-element model for hysteresis and its steady-state dynamic response. Trans ASME J Appl Mech. https://doi.org/10.1115/1.3625199
41. Armstrong-Hélouvry B (1991) Control of machines with friction. Kluver Academic Publishers, London
42. Čepon G, Manin L, Boltežar M (2010) Experimental identification of the contact parameters between a V-ribbed belt and a pulley. Mech Mach Theory 45:1424–1433. https://doi.org/10.1016/j.mechmachtheory.2010.05.006
43. Čepon G, Manin L, Boltežar M (2009) Introduction of damping into the flexible multibody belt-drive model: a numerical and experimental investigation. J Sound Vib 324:283–296. https://doi.org/10.1016/j.jsv.2009.02.001
44. Pfeiffer F (1991) Dynamical systems with time-varying or unstedy structure. ZAMM—Zeitschrift für angewandte Mathematik und Mechanik, Bd. 71, No.4
45. Wojciech S (1995) Dynamic analysis of manipulators with consideration of dry friction. Comput Struct 57(6):1040–1050